Precipitation Processes in Al-Cu-Mg Alloys Microalloyed with Si

C.R. HUTCHINSON and S.P. RINGER

Microalloying additions of Si are known to increase significantly the response to age hardening of 2xxx series Al-Cu-Mg alloys, and commercial alloys such as 2618 are based on this effect. Previous work has attributed this effect to a refined dispersion of S′ or S phase (Al_2CuMg) precipitates. This work reports the results of a detailed microstructural characterization, employing transmission electron microscopy–based techniques, on the effects of Si additions to a base Al-2.5Cu-1.5Mg (wt pct) alloy. It was found that the peak hardness microstructure contains a fine and uniform dispersion of Si-modified Guinier-Preston-Bagaratsky (GPB) zones. These zones are lath shaped, possessing $\{100\}_\alpha$ facets, elongated along $\langle 100\rangle_\alpha$ directions and contain Si. The S phase was also observed at peak hardness, although it is concluded that these precipitates do not contribute significantly to hardening due to their coarse dispersion, which arises from their heterogeneous nucleation on the quenched-in defect structure. Overaging was associated with the replacement of the zones by the S phase through a process involving dissolution and reprecipitation together with heterogeneous nucleation of S at the zones. The precipitation of θ' (Al_2Cu) and σ ($Al_5Cu_6Mg_2$) phase was also observed in alloys containing $\geq$0.5 wt pct Si. It is demonstrated that the total solute content of the alloy has a major influence on the precipitation reactions during aging.

I. INTRODUCTION

ALLOYS of the Al-Cu-Mg system form an important part of the 2xxx series alloys and are widely used in structural aerospace applications. Moreover, this system provides the basis for the development of many other important Al alloys. An important example includes Si-modified alloys having compositions that lie in the (α + S) region of the experimentally derived Al-Cu-Mg phase diagram proposed by Brook,[1] which have application in skin sections and rivet components of supersonic jet aircraft. Alloy 2618 is based on Al-3Cu-3Mg-0.5Si (wt pct) and was originally developed for the Concorde superstructure. Although additions of Si are associated with improved tensile and creep strengths, details of the precise mechanism by which Si enhances hardening and refines microstructure remain unclear. Renewed interest in this system was stimulated by studies of the rapid hardening that occurs in base Al-Cu-Mg alloys[2–6] and the observation that this effect is enhanced in Si-bearing alloys.[2,7]

The precipitation sequence observed during elevated temperature aging of Al-Cu-Mg alloys in the (α + S) region depends on the Cu/Mg ratio. For a Cu/Mg weight ratio of 2.2, Bagaryatsky[8,9] reported the following precipitation sequence.

$$\text{Supersaturated solid solution} \rightarrow \text{GPB zones} \rightarrow S'' \rightarrow S' \rightarrow S.$$

The Guinier-Preston (GP) zone structures in these alloys were designated as Guinier-Preston-Bagaratsky (GPB) zones by Silcock,[10] who showed that they possess a rod-shaped morphology extended along the cube directions of the α matrix. Recent three-dimensional atom probe (3DAP) work by Reich *et al.*[6] indicates that they are composed of Cu and Mg atoms and that their formation is preceded by the formation of more diffuse Cu-Mg coclusters. Despite reports of the S″ phase by Bagaryatsky,[8,9] Cuisat *et al.*,[11] Zahra *et al.*,[12,13] and Ratchev *et al.*,[5] it is noteworthy that Silcock,[10] Wilson and Partridge,[7] Jena *et al.*,[14] and Ringer *et al.*[3,4] were unable to confirm the presence of the S″ phase. The S″ and S′ phases are proposed to be precursors to the equilibrium S phase (Al_2CuMg, *Cmcm*, a = 0.400 nm, b = 0.923 nm, and c = 0.714 nm).[15] There is now thought to be little difference between the S′ and S phases,[3,6,16] which occur as lath-shaped precipitates on $\{210\}_\alpha$ planes elongated along $\langle 100\rangle_\alpha$. High resolution transmission electron microscopy (HRTEM)[17] and microbeam electron diffraction (MBED)[18] have revealed that the habit plane of the lath-shaped S-phase precipitates is $(001)_s$, oriented such that $(100)_s // \{100\}_\alpha$ and $[010]_s // \langle 012\rangle_\alpha$. It is noteworthy that slight rotations from the preceding orientation relationship have been reported[18] and that the distribution and morphology of the S phase do vary. In a study of an Al-2.5Cu-1.2Mg (wt pct) alloy aged artificially at 190 °C, Wilson and Partridge[7] found that the S′(S) precipitates nucleated heterogeneously on quenched-in dislocation loops and helices, forming corrugated sheets on $\{210\}_\alpha$ planes. In subsequent work, Gupta *et al.*[16] examined an alloy with a similar Cu/Mg ratio but lower total solute content. They found that aging of an Al-1.53Cu-0.79Mg (wt pct) alloy at 190 °C resulted in rod-shaped S′(S) precipitates and concluded that the total solute content of the alloy influences the precipitate morphology.

There have been several studies on the effects of microalloying with Si on precipitation processes in Al-Cu-Mg alloys. Vietz and Polmear[2] observed an enhanced response to age hardening at elevated temperatures in Al-2.5Cu-1.5Mg (wt pct) with additions of 0.25 (wt pct) Si. It was

C.R. HUTCHINSON, formerly student at Monash University, is postgraduate student, Department of Materials Science and Engineering, University of Virginia, Charlottesville, VA 22903, USA. S.P. RINGER, formerly Associate Professor of the Department of Materials Engineering at Monash University, is now Director of the Electron Microscope Unit at the University of Sydney, NSW, 2006, Australia.

Manuscript submitted January 17, 2000.

found that the presence of Si raised the level of hardening over the entire time scale. Times to peak hardness were unaltered and it was proposed that Si affected only the first stage of hardening. In a study of the effects of 0.25 (wt pct) Si additions on age hardening of Al-2.5Cu-1.2Mg (wt pct), Wilson *et al.*[19] showed that the room temperature age-hardening response was delayed and the elevated temperature response enhanced by the Si additions. It was reported that the rate of formation of GPB zones at room temperature was less in the Si-bearing alloy and that the dispersion of S′(S) precipitates formed at elevated temperatures was finer and more uniform. The depressed room temperature response to age hardening of the Si-containing alloy was interpreted as a preferred interaction between Si atoms and vacancies. Wilson[20] found that the presence of 0.24 wt pct Si in solid solution caused the quenched-in dislocation loops and helices to be smaller and fewer than in the Si free ternary alloy. This was consistent with the observations by Weatherly and Nicholson[21,22] (reported by Wilson *et al.*[19]) on an Al-2.7Cu-1.35Mg-0.2Si (wt pct) alloy. Wilson *et al.* attributed the refined distribution of S′(S) to the influence of Si on the defect structure and the formation of GPB zones. First, the reduced number of dislocation loops and helices in the as-quenched (AQ) Si-containing alloys provided fewer heterogeneous nucleation sites for S′(S). Second, the increased stability of GPB zones was attributed to their modification by Si, which was proposed to inhibit the nucleation and growth of S′. Weatherly and Nicholson[22] found that Si had little effect on the length of S′ precipitates but greatly reduced the cross-sectional area in an Al-2.7Cu-1.35Mg-0.2Si (wt pct) alloy aged at 260 °C.

In contrast with the observations of Wilson and co-workers,[7,19,20] Suzuki *et al.*[23] suggests an entirely different precipitation sequence, which results in the formation of S′(S), β' (Mg_2Si), and an unknown X phase in the alloy Al-2Cu-0.9Mg-0.25Si (wt pct). Furthermore, Suzuki *et al.* proposed that the addition of 0.5 wt pct Si promotes the precipitation of θ' (Al_2Cu), X, and Q ($Al_5Cu_2Mg_8Si_6$) and suppresses the formation of S′(S) and β'. More recently, Gupta *et al.*[24,25] and Jena *et al.*[26] studied the effect of 0.23, 0.49, 0.76, and 1.03 wt pct additions of Si to Al-1.52Cu-0.75Mg (wt pct). These alloys contain a lower total solute content than the alloys studied by Suzuki *et al.* and by Wilson and co-workers.[7,19,20] This work showed that additions greater than 0.23 wt pct resulted in the formation of the insoluble compound Q ($Al_5Cu_2Mg_8Si_6$). The large differences in the reported precipitation sequence between additions of 0.23 and 0.5 wt pct Si to the Al-Cu-Mg alloys were interpreted in terms of the effect of the formation of Q phase on the composition of the matrix. On the basis of differential scanning calorimetry, Gupta *et al.*[25] also concluded that Si was bound preferentially with GPB zones. The precipitation of S′(S) was confirmed by transmission electron microscopy (TEM) and the effects of 0.23 wt pct Si on the precipitation sequence were in agreement with the observations of Wilson and co-workers.[7,19,20] In a related study, Chaturvedi *et al.*,[27] using the same alloy as Gupta *et al.* concluded that the presence of 0.23 wt pct Si in Al-1.52Cu-0.74Mg (wt pct) does not alter the sequence, structure, or distribution of the precipitating phase, but reduces the activation energy for GPB zone formation. The studies of Gupta and co-workers, Wilson *et al.*, and Suzuki *et al.* suggest that the effect of microalloying with Si to Al-Cu-Mg alloys may not only depend on the Cu/Mg ratio but also on the total solute content of the alloy.

Table I. Alloys Used in the Present Study

Alloy Designation	Composition (Wt Pct)	Composition (At. Pct)
1	Al-2.5Cu-1.5Mg	Al-1.1Cu-1.7Mg
2	Al-2.5Cu-1.5Mg-0.1Si	Al-1.1Cu-1.7Mg-0.1Si
3	Al-2.5Cu-1.5Mg-0.25Si	Al-1.1Cu-1.7Mg-0.25Si
4	Al-2.5Cu-1.5Mg-0.5Si	Al-1.1Cu-1.7Mg-0.5Si

In summary, there are a number of uncertainties in the microstructural evolution in Al-Cu-Mg-Si alloys. First, the results of Wilson and co-workers and Suzuki *et al.* suggest an apparent conflict in the identity of which precipitates are stimulated by Si additions to alloys with similar Cu/Mg ratios and total solute contents. Second, it remains to confirm using high resolution techniques whether the effect of Si additions is to refine the distribution of the S phase, as reported by Wilson and co-workers.[7,19,20] Furthermore, the potential mechanism underlying this refinement remains to be clarified. Similarly, various precipitates reported by Wilson *et al.* and Weatherly and Nicholson[21,22] in alloys containing 0.25 wt. pct Si and by Suzuki *et al.* and Gupta *et al.* in the alloys containing 0.5 wt pct Si or greater remain unidentified. Finally, the work of Wilson and Partridge[7] in ternary Al-Cu-Mg alloys suggested that the morphology adopted by S′(S) and the precipitation sequence depend on the total solute content of the alloy. It remains to establish whether this is also the case for the Si-containing alloys and, if so, if it can account for the differences in the experimental observations reported so far. This article addresses these questions through direct characterization using TEM-based techniques on a set of alloys containing systematic additions of Si to a base Al-2.5Cu-1.5Mg wt pct.

II. EXPERIMENTAL PROCEDURE

Systematic additions of 0.1, 0.25, and 0.5 wt pct Si were made to a base alloy composition of Al-2.5Cu-1.5Mg (wt pct) (Table 1). The alloys were cast into book molds, homogenized, and scalped. The samples were solution treated in a salt bath at 525 °C ± 2 °C for 1 hour followed by immediate quenching into cold water. In the case of elevated temperature aging, the samples were immediately placed into a salt bath at 200 °C ± 1 °C. Samples undergoing room temperature aging were stored at a temperature of ~ 20 °C. The age-hardening response of these alloys was monitored by Vickers hardness measurements (VHN) using a 5-kg load. The microstructural changes in the alloys were examined using scanning electron microscopy (SEM), conventional transmission electron microscopy (CTEM), and HRTEM. Samples for SEM were prepared by standard metallographic techniques and examined using a JEOL* JSM-840A scanning electron microscope operating at 20 kV. Energy dispersive X-ray spectroscopy (EDXS) was conducted in the SEM using a TRACOR-NORTHERN** microanalysis system

*JEOL is a trademark of Japan Electron Optics Ltd., Tokoyo.

**TRACOR-NORTHERN is a trademark of Noran Instruments, Inc., Middleton, WI.

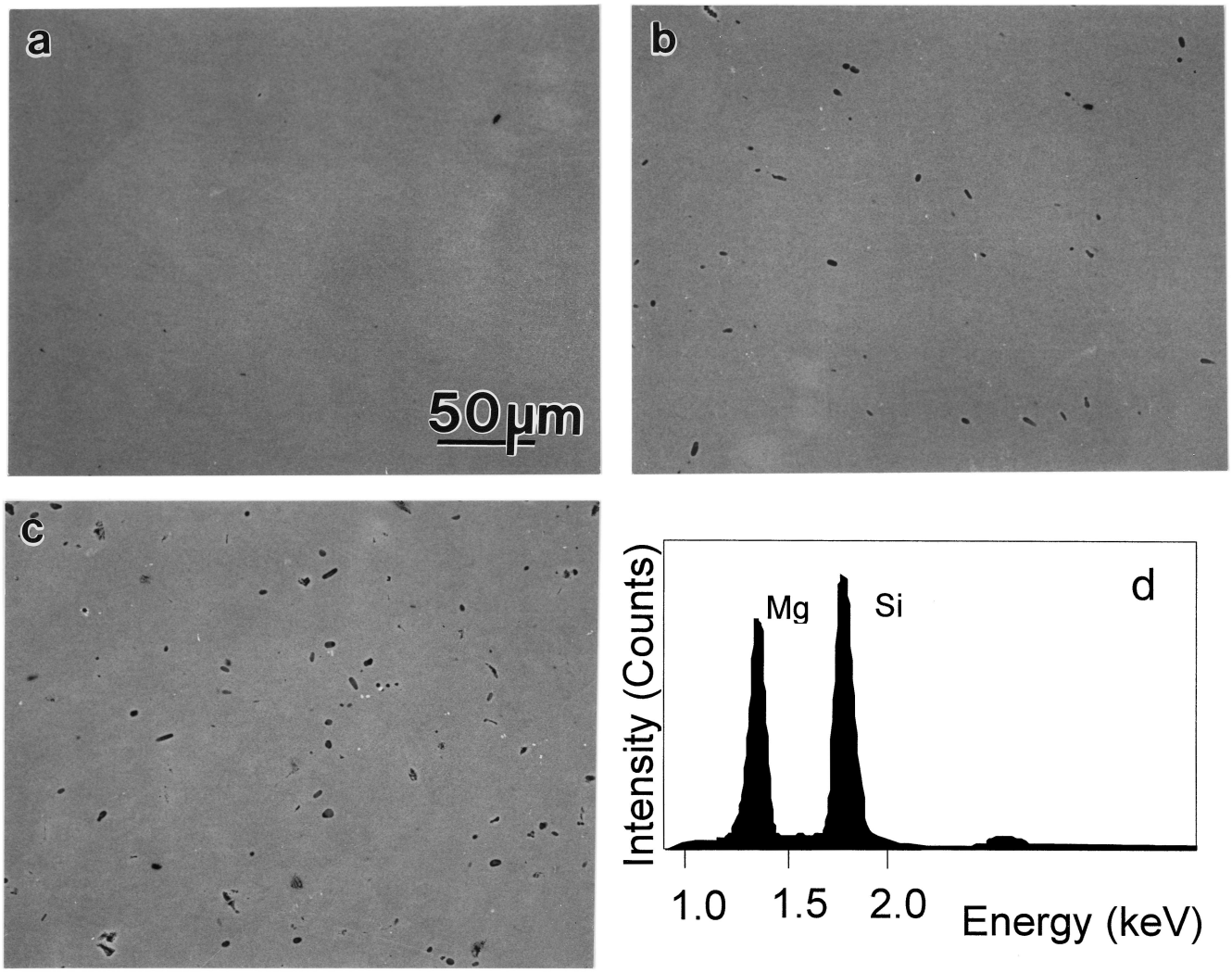

Fig. 1—Electron backscattered images of (*a*) Al-2.5Cu-1.5Mg-0.1Si, (*b*) Al-2.5Cu-1.5Mg-0.25Si, and (*c*) Al-2.5Cu-1.5Mg-0.5Si (wt pct) in the AQ condition. An energy dispersive X-ray spectrographic trace from an insoluble particle in the alloy containing 0.5 (wt pct) Si is provided in (*d*).

operating at 8 kV. The choice of 8 kV was made on the basis of Monte Carlo simulations of the interaction volume of the electron probe to ensure that chemical information was obtained exclusively from the precipitates and not from the underlying matrix. Thin foils for TEM were prepared by standard techniques and examined using either a PHILIPS† CM-20 microscope or a JEOL JEM-2000FXII both operating at 200 kV. Examination of the AQ specimens was performed within 1 hour of quenching. Furthermore, to facilitate meaningful qualitative comparisons between the defect structures in the as-quenched and naturally aged microstructures, considerable care was taken to obtain representative micrographs away from the edge of the foil. Two-beam conditions were used to obtain thickness fringes so that images could be recorded from regions of constant thickness. The HRTEM was performed on a JEOL JEM-4000EX operating at 400 kV and energy-dispersive X-ray spectroscopy (EDXS) analysis in the TEM was carried out using a JEOL JEM-2010F operating at 200 kV equipped with a field emission gun and an Oxford EDXS system.

†PHILIPS is a trademark of Philips Electronic Instruments Corp. Mahwah, NJ.

Table II. Volume Fraction of Insoluble Mg_2Si Particles (at the 95 Pct Confidence Level)

Alloy (Wt Pct)	Volume Fraction in AQ Condition	Volume Fraction after Aging at 200 °C for 7 Days
Al-2.5Cu-1.5Mg-0.1Si	0.22 ± 0.15 pct	0.30 ± 0.18 pct
Al-2.5Cu-1.5Mg-0.25Si	0.44 ± 0.17 pct	0.97 ± 0.31 pct
Al-2.5Cu-1.5Mg-0.5Si	0.81 ± 0.25 pct	1.05 ± 0.30 pct

III. RESULTS

A. *AQ Microstructures*

Examination of the AQ microstructures by SEM indicated that the ternary Al-2.5Cu-1.5Mg (wt pct) alloy was single phase; however, the Si-containing alloys contained insoluble constituents (Figure 1). The density of these constituents was determined by standard point counting techniques,[28] and the respective volume fractions at the 95 pct confidence level are summarized in Table II. The volume fraction of constituents was found to increase with Si content.

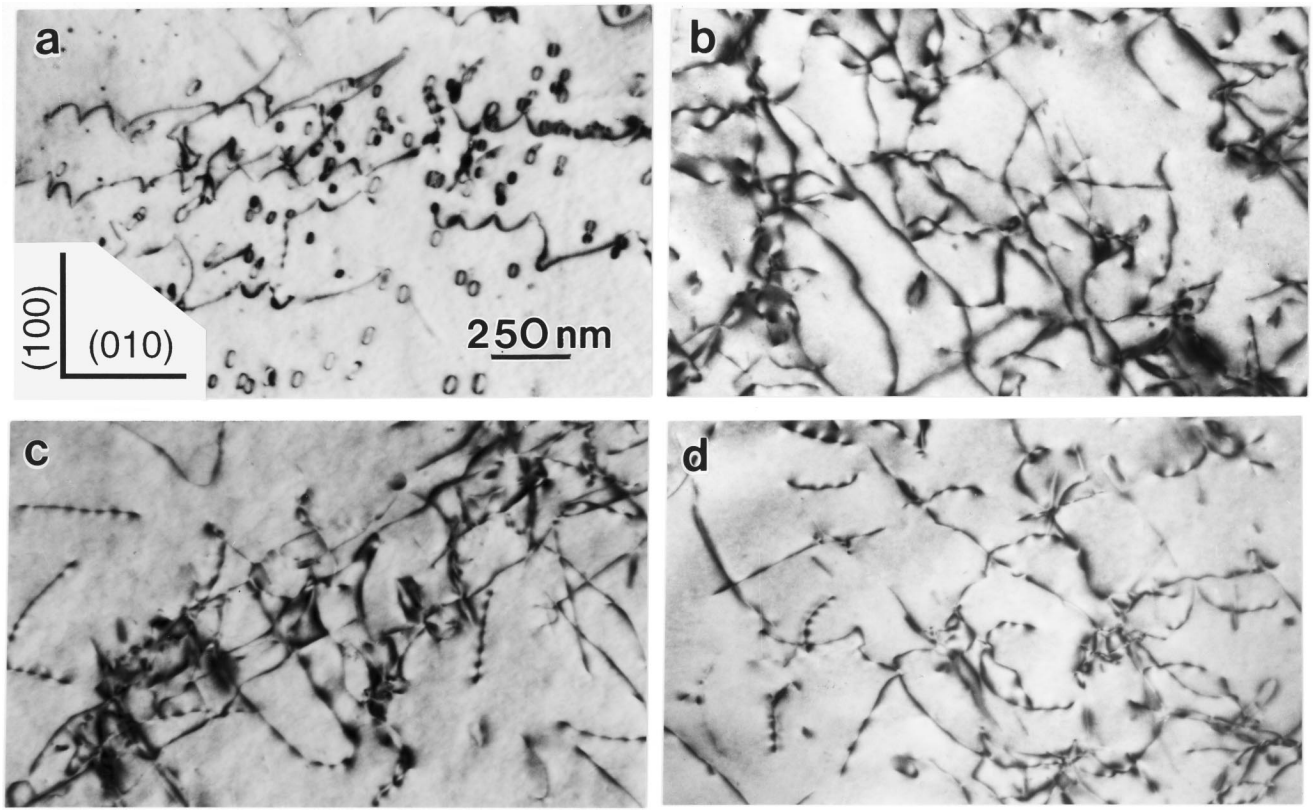

Fig. 2—BF transmission electron micrographs recorded near the $\langle 001 \rangle_\alpha$ orientation from the AQ microstructure of the (*a*) base Al-2.5Cu-1.5Mg, (*b*) Al-2.5Cu-1.5Mg-0.1Si, (*c*) Al-2.5Cu-1.5Mg-0.25Si, and (*d*) Al-2.5Cu-1.5Mg-0.5Si (wt pct) alloys.

In SEM backscatter mode, these constituents image darker than the surrounding matrix, indicating a lower average atomic weight. Figure 1(d) is a representative EDXS spectrum obtained from these constituents and serves to indicate that they consist exclusively of Si and Mg. The dark nature of these constituents and the absorption of Mg, which would need to be corrected for in a quantitative analysis of the composition of these constituents, indicates that these are Mg-rich constituents. On the basis of these observations, these constituents were tentatively identified as Mg_2Si. Occasionally, white constituents were also observed. These were found to be pure Si.

Figure 2 shows bright-field (BF) TEM micrographs recorded near the $\langle 001 \rangle_\alpha$ zone axis of each alloy in the AQ condition. The BF image of the ternary alloy (Figure 2(a)) shows the formation of both dislocation loops and helices and there was no evidence of precipitation. In contrast, dislocation loops were generally absent from the microstructure of the Si-containing alloys, which contained dislocation helices. Again, there was no evidence of fine-scale precipitation. The AQ hardness for each alloy is summarized in Table III. It is seen that the hardness of the Si-containing alloys in the AQ condition decreased with increasing Si content. The selected area electron diffraction (SAED) patterns recorded for each alloy in the AQ condition (not reproduced here) only exhibited reflections from the matrix.

B. *Naturally Aged Alloys*

1. *Hardening*

The hardness-time curves for each alloy following aging at room temperature (natural aging) are provided in Figure 3. Each of the alloys exhibited similarly shaped curves, with an initial period of constant hardness from the AQ state before rising to a plateau within 200 hours. The aging response of the microalloyed specimens falls into a band that exhibits a delayed response to hardening and a lower hardness than the ternary alloy at all times monitored.

2. *Microstructural examination*

Figure 4 provides a series of BF TEM micrographs recorded near the $\langle 001 \rangle_\alpha$ zone axis for each alloy after natural aging for 400 days. The ternary alloy (Figure 4(a)) shows a large increase in dislocation loop density, and growth of the loops is evident when their size is compared to that observed in the AQ condition. Following careful examination, we were unable to discern diffraction effects in the corresponding SAED patterns other than those arising from the matrix or surface oxide films. Similarly, contrast from precipitates was not observed in the BF images.

The BF TEM images of the Si-containing quaternary alloys show the growth of dislocation helices and, unlike the ternary alloy, a general absence of dislocation loops from the microstructures. The growth of helical dislocations appears to be along $\langle 110 \rangle_\alpha$ directions (Figures 2(b) and (c)); however, growth of helices in $\langle 001 \rangle_\alpha$ directions was also observed with increasing frequency in alloys with higher Si content (Figure 4(d)). Wilson *et al.*[19,20] also observed growth of dislocations along matrix $\langle 100 \rangle_\alpha$ directions and speculated that it may be due to pinning of the screw dislocation by Si atoms along its length. There was no precipitation apparent in the BF images of the quaternary Si-containing alloys.

Table III. Changes in Hardness (VHN) during Aging at 200 °C

Wt Pct	Alloy 1 Al-2.5Cu-1.5Mg	Alloy 2 Al-2.5Cu-1.5Mg-0.1Si	Alloy 3 Al-2.5Cu-1.5Mg-0.25Si	Alloy 4 Al-2.5Cu-1.5Mg-0.5Si
AQ hardness	61.3	57	55.8	54.5
2 min hardness	88.2	106.4	107.2	104.5
2 min hardness-AQ hardness	26.9	49.4	51.4	50
Peak hardness	116.2	134.5	145	146
Peak hardness-AQ hardness	54.9	77.5	89.2	91.5
2 min hardness/peak hardness	0.76	0.79	0.74	0.72
(2 min-AQ)/(Peak-AQ)	0.49	0.64	0.58	0.55

"2 min" denotes the hardness after aging for 2 min at 200 °C and "Peak" denotes peak hardness at 200 °C.

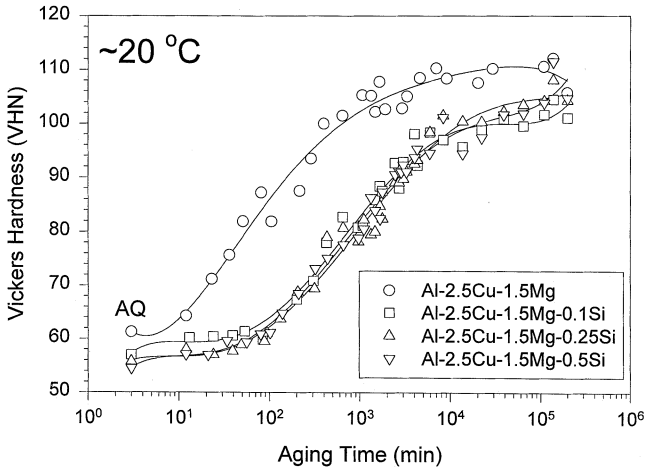

Fig. 3—Room temperature (natural aging) hardness-time curves for the Al-2.5Cu-1.5Mg-(Si) (wt pct) alloys studied.

C. *Aging at 200 °C*

1. *Hardening*

Figure 5 is a hardness-time curve containing data for each of the alloys after aging at 200 °C. All alloys exhibited two stages of hardening, the first of which was complete within seconds of exposure at the aging temperature. Each of the Si-containing alloys exhibits an enhanced age-hardening response, and it is particularly noteworthy that the hardness increment associated with the initial rapid hardening was almost double that observed in the ternary alloy. The second stage of hardening for the Si-containing alloys involved a relatively steady rise to peak hardness followed by overaging. The peak hardness increased with Si content as did the rate of decline in hardness associated with overaging. The changes in hardness associated with each of the alloys at 200 °C are summarized in Table III.

2. *Microstructural examination*

Following recent work on the clustering, precipitation, and hardening processes in the ternary alloy,[3–6] a detailed microstructural examination was made for each of the Si-containing alloys. Figures 6 through 8 are BF TEM micrographs recorded near the $\langle 001 \rangle_\alpha$ zone axis and include the corresponding SAED patterns, respectively, in (a) underaged, (b) peak-hardness, and (c) overaged (7 days) conditions.

a. *Underaged (5 minutes at 200 °C)*

The BF TEM micrographs for each of the Si-containing alloys show signs of very fine precipitation, the density of which increased with Si content. This is indicated in the SAED patterns, where streaking through $\{010\}_\alpha$ positions in $\langle 001 \rangle_\alpha$ directions increases in intensity with increasing Si content. These effects are typical of the shape effect from GPB zones elongated along $\langle 001 \rangle_\alpha$ directions, and the BF images in Figures 6 through 8 show the variants parallel to the electron beam, in the end-on orientation. Finally, it is noted that the underaged microstructures retained a dense distribution of the quenched-in defects, although the contrast conditions in the micrographs presented in Figures 6(a),7(a), and 8(a) were selected to emphasize the fine scale precipitation.

b. *Peak hardness (10 hours at 200 °C for Al-2.5Cu-1.5Mg-0.1Si; 14 hours at 200 °C for Al-2.5Cu-1.5Mg-0.25Si; and 20 h at 200 °C for Al-2.5Cu-1.5Mg-0.5Si)*

The peak hardness microstructures for each of the Si-containing alloys is dominated by a very fine and uniform distribution of lath-shaped Si-modified GPB zones. The fine scale precipitation has been termed "Si-modified GPB zones" so as to emphasize their obvious similarity to the GPB zones that form in ternary Al-Cu-Mg alloys. Although compositional and morphological differences between these precipitate phases are reported subsequently, these do not seem to warrant the introduction of a unique or new nomenclature. For example, when viewed at higher magnifications, as provided in the inset micrographs, these zones appeared to exhibit $\{001\}_\alpha$ facets, which is distinct from the almost equiaxed cross section reported for GPB zons in Al-Cu-Mg alloys.[3–10] Heterogeneous precipitation of the S phase is also apparent on dislocation helices, formed from the quenched-in defect structure. In the vicinity of the S-phase precipitates, regions free of precipitation of the Si-modified GPB zones were observed. Similar observations were recently reported for the base ternary Al-2.5Cu-1.5Mg wt pct alloy,[6] and this is interpreted as indirect evidence for a preferred solute-dislocation interaction, which precedes formation of the Si-modified GPB zones. The SAED patterns exhibited very sharp and obvious streaking in $\langle 001 \rangle_\alpha$ directions through the $\{010\}_\alpha$ positions in reciprocal space. These are characteristic of well-defined precipitates elongated in $\langle 001 \rangle_\alpha$ directions in the matrix.

A more detailed examination of the peak hardness microstructures was undertaken using HRTEM, and Figures 9 and 10 feature results from the Al-2.5Cu-1.5Mg-0.25Si (wt pct) alloy, which were typical for all the Si-containing alloys studied. Figure 9(a) is an HRTEM micrograph recorded with the electron beam parallel to $\langle 001 \rangle_\alpha$ and demonstrates the lack of periodic order in the Si-modified GPB zones that

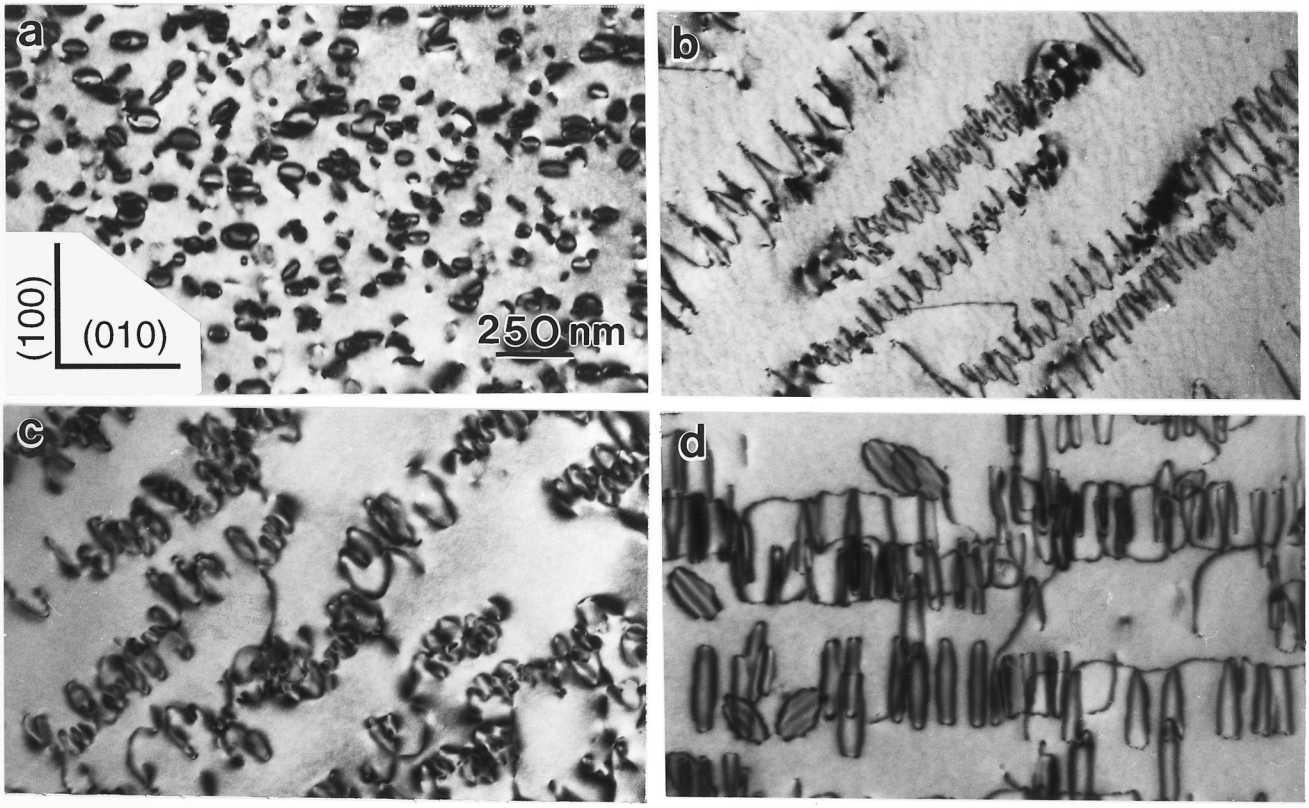

Fig. 4—BF transmission electron recorded near the $\langle 001 \rangle_\alpha$ orientation from the (*a*) base Al-2.5Cu-1.5Mg, (*b*) Al-2.5Cu-1.5Mg-0.1Si, (*c*) Al-2.5Cu-1.5Mg-0. 25Si, and (*d*) Al-2.5Cu-1.5Mg-0.5Si (wt pct) alloys in the naturally aged condition (400 days, 20 °C).

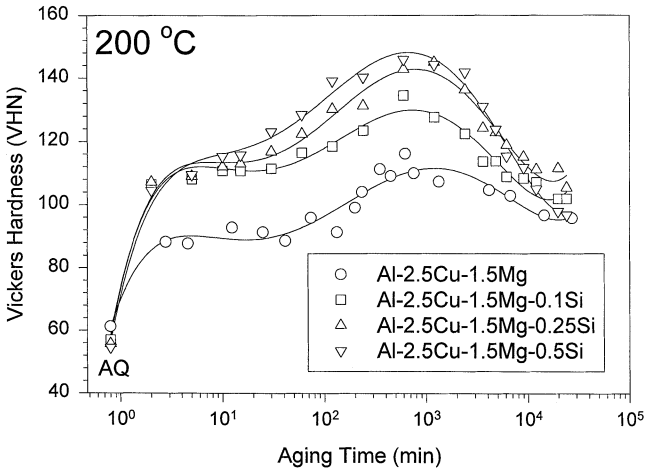

Fig. 5—Hardness-time curves for the Al-2.5Cu-1.5Mg-(Si) (wt pct) alloys studied (200 °C).

dominate the peak hardness microstructures in each of the Si-containing alloys. Figure 9(b) is an EDXS spectrum taken from a typical rodlike zone using a field emission gun (FEG) TEM with a 0.7-nm probe, and Figure 9(c) is a comparative analysis from a nearby region in the matrix. The spectra show the presence of Cu, Mg, Al, and Si in addition to the C peak due to contamination from such a finely focused electron probe and a small O peak from the oxide layer formed near the perforation in the thin foil. The analysis shows clearly that the GPB zones contain Si and Mg. The presence of Si within these zones has influenced their morphology, since facets parallel to $\{001\}_\alpha$ planes are clearly observed in Figure 9(a). Two variants of this morphology are distinguished in Figure 9, suggesting that there may be a total of at least six variants. The crystallographic relationship between the lath-shaped zone structure and the matrix does not appear to change with Si content. All zones in all alloys were elongated along $\langle 001 \rangle_\alpha$ directions, although the cross-sectional morphology did change from an approximately square rod in the 0.1 wt pct Si alloy to a higher aspect ratio lath shape in the higher Si alloys.

Figure 10 is an HRTEM micrograph recorded with the electron beam parallel to $\langle 001 \rangle_\alpha$ showing what may be interpreted as the heterogeneous nucleation of S phase in the strain field of or on one of the Si-modified GPB zones. At this scale, the zones are significantly spaced, suggesting that the likelihood of this micrograph being a case of coincidental impingement is very small. Each of the Si-containing alloys contains a dense distribution of GPB-like rod or lath-shaped zones in the peak-aged microstructure and coarsens into a microstructure of uniformly distributed S phase. The heterogeneous nucleation of S phase on the zones seems a plausible mechanism for the refined distribution of S observed in the overaged microstructures. A refined distribution of S phase, as had previously been reported, was not observed in the peak hardness microstructures in any of the Si-containing alloys.

c. *Overaged (7 days at 200 °C)*

The overaged microstructures show the development of an increasingly uniform distribution of the S phase at the

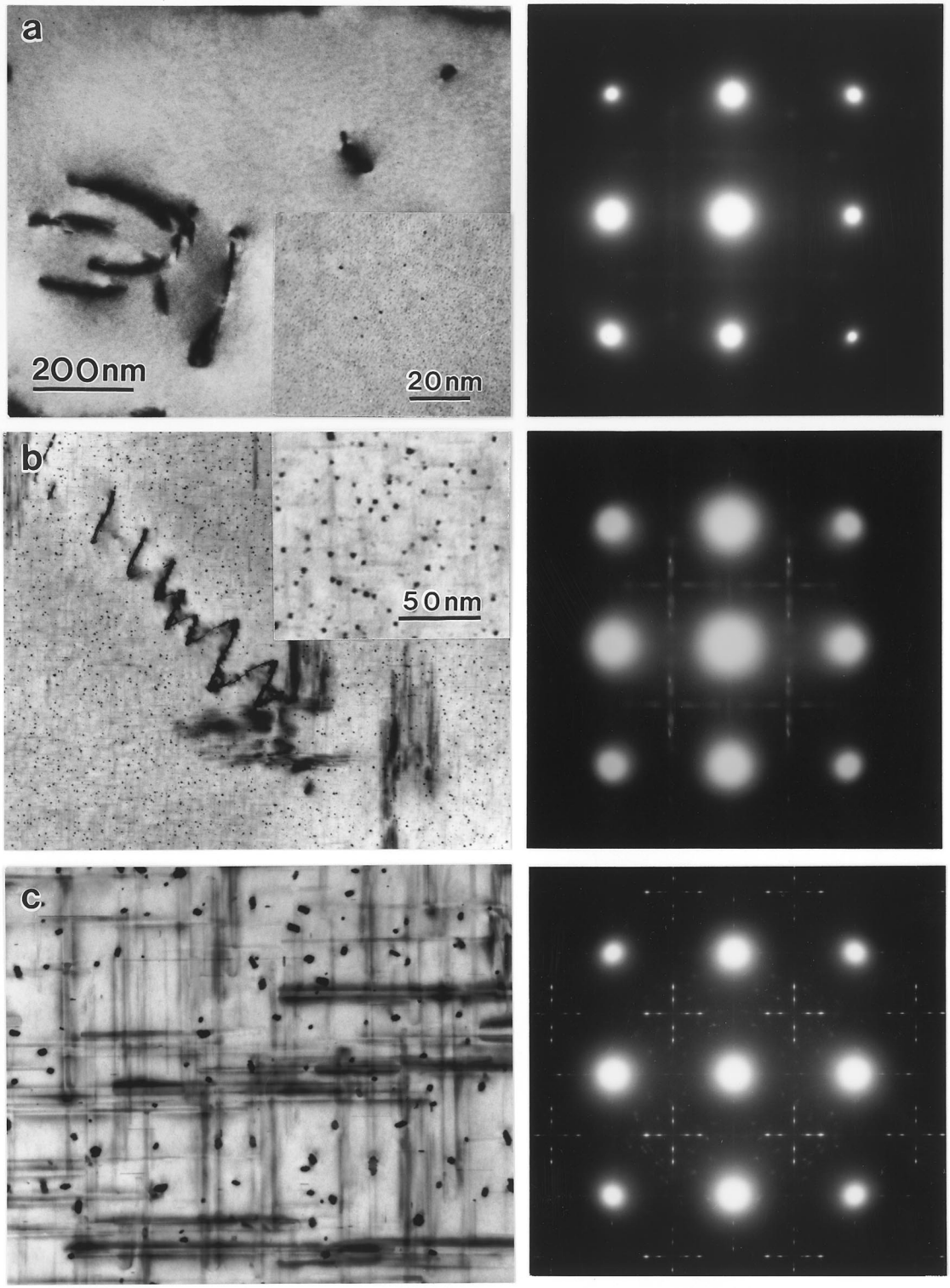

Fig. 6—BF transmission electron micrographs and corresponding selected area electron diffraction patterns recorded near the $\langle 001 \rangle_\alpha$ orientation from the Al-2.5Cu-1.5Mg-0.1Si (wt pct) alloy in the (*a*) underaged: 200 °C, 5 min; (*b*) peak hardness: 200 °C, 10 h; and (*c*) overaged: 200 °C, 7 days conditions.

expense of the rod and lath-shaped GPB zone–like precipitates resolved in the peak-hardness microstructure. The SAED patterns of the alloys containing 0.1 and 0.25 Si wt pct Si show the archetypal reflections from the S phase. The SAED patterns show the characteristic crosses about the forbidden $\{110\}_\alpha$ reflections, but they also show an array of much weaker reflections. The S precipitate forms 12 crystallographic variants with the aluminum matrix, and it has recently been shown that the intense reflections in the cross about the forbidden $\{110\}_\alpha$ reflections arise from the eight variants with $[100]_S || [100]_\alpha$ or $[100]_S || [010]_\alpha$, while the faint reflections arise from the four variants with $[100]_S || [001]_\alpha$.[16] Two additional precipitate phases were observed in the alloy containing 0.5 wt pct Si and these are featured

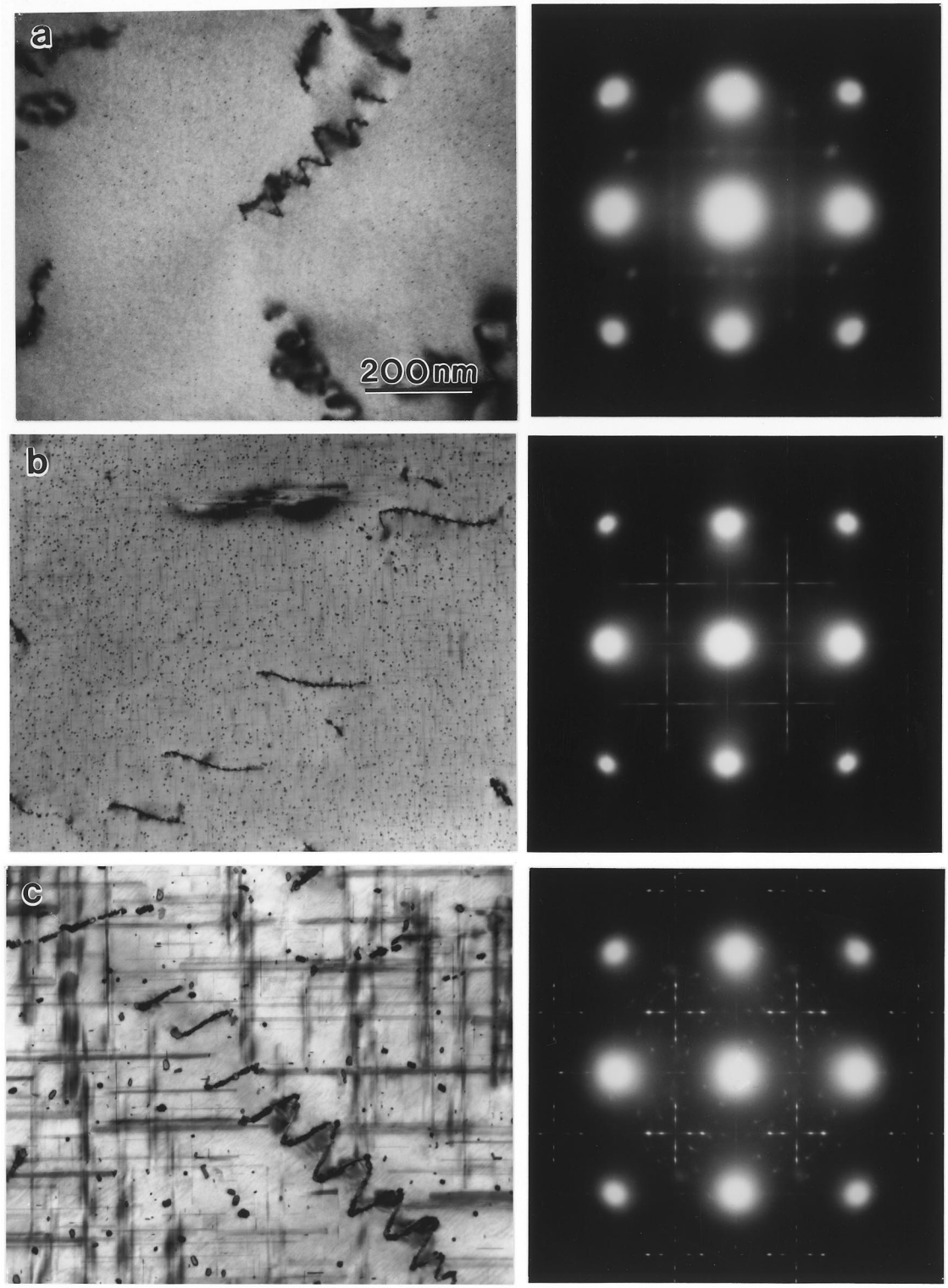

Fig. 7—BF transmission electron micrographs and corresponding selected area electron diffraction patterns recorded near the $\langle 001 \rangle_\alpha$ orientation from the Al-2.5Cu-1.5Mg-0.25Si (wt pct) alloy in the (*a*) underaged: 200 °C, 5 min; (*b*) peak hardness: 200 °C, 14 h; and (*c*) overaged: 200 °C, 7 days conditions.

in Figure 11. The precipitates arrowed in Figure 11(a) exhibit a cuboidal morphology with traces parallel to the cube planes of the matrix, and these were identified as the cubic σ phase ($P3m$, $a = 0.831$ nm, $Al_5Cu_6Mg_2$)[29] by MBED (Figure 11(b)). It is likely that these are the same cubic precipitates observed by Wilson[20] and by Weatherly and Nicholson.[21,22] Furthermore, platelike precipitates were observed, and evidence of this is provided in Figure 11(c). The observation of these precipitates, which were identified through MBED as θ' (Figure 11(d)), concurs with the observations by Suzuki *et al.*[23] The volume fraction of the insoluble Mg_2Si particles observed in the AQ microstructures (Figure 1) was also measured in the overaged condition (Table II). The composition of this phase was not observed to change;

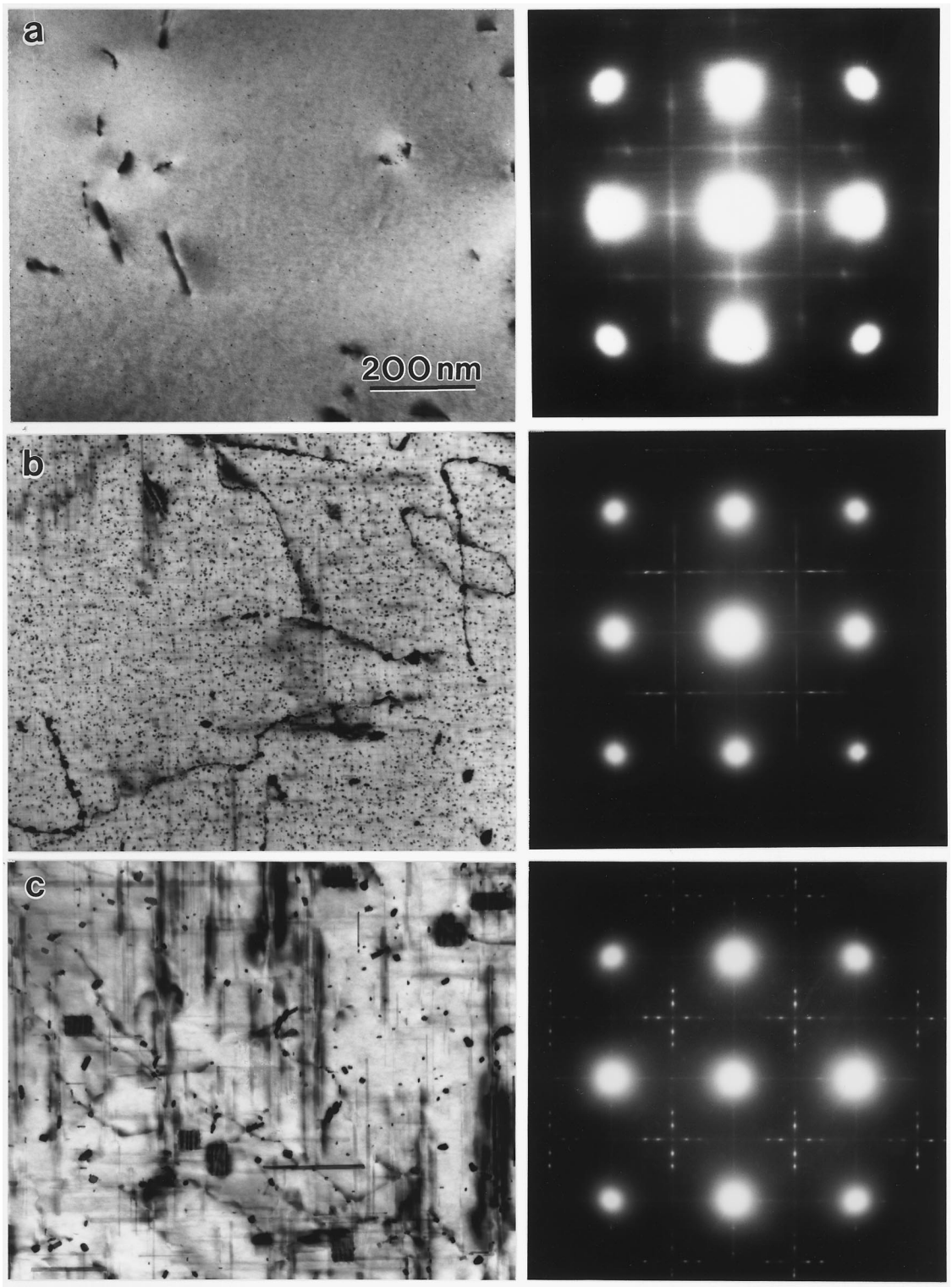

Fig. 8—Bright-field transmission electron micrographs and corresponding SAED patterns recorded near the $\langle 001 \rangle_\alpha$ orientation from the Al-2.5Cu-1.5Mg-0.5Si (wt pct) alloy in the (*a*) underaged: 200 °C, 5 min; (*b*) peak hardness: 200 °C, 20 h; and (*c*) overaged: 200 °C, 7 days conditions.

however, the volume fractions did increase, indicating that progressively more Mg was removed from the solid solution during aging at 200 °C.

IV. DISCUSSION

The presence of insoluble Mg_2Si particles in alloys containing as little as 0.1 wt pct Si may be compared with the results of Gupta *et al.*, who reported a solubility of 0.3 wt pct Si in an Al-1.52Cu-0.75Mg wt pct alloy at 530 °C.[24,25] An isotherm at 520 °C, constructed by Collins,[30] provides valuable insight into the reported precipitation sequences for Al-Cu-Mg-Si alloys with the same Cu/Mg ratio yet different total solute contents. Collins prepared 48 Al-Cu-Mg-Si alloys of various compositions and used the available

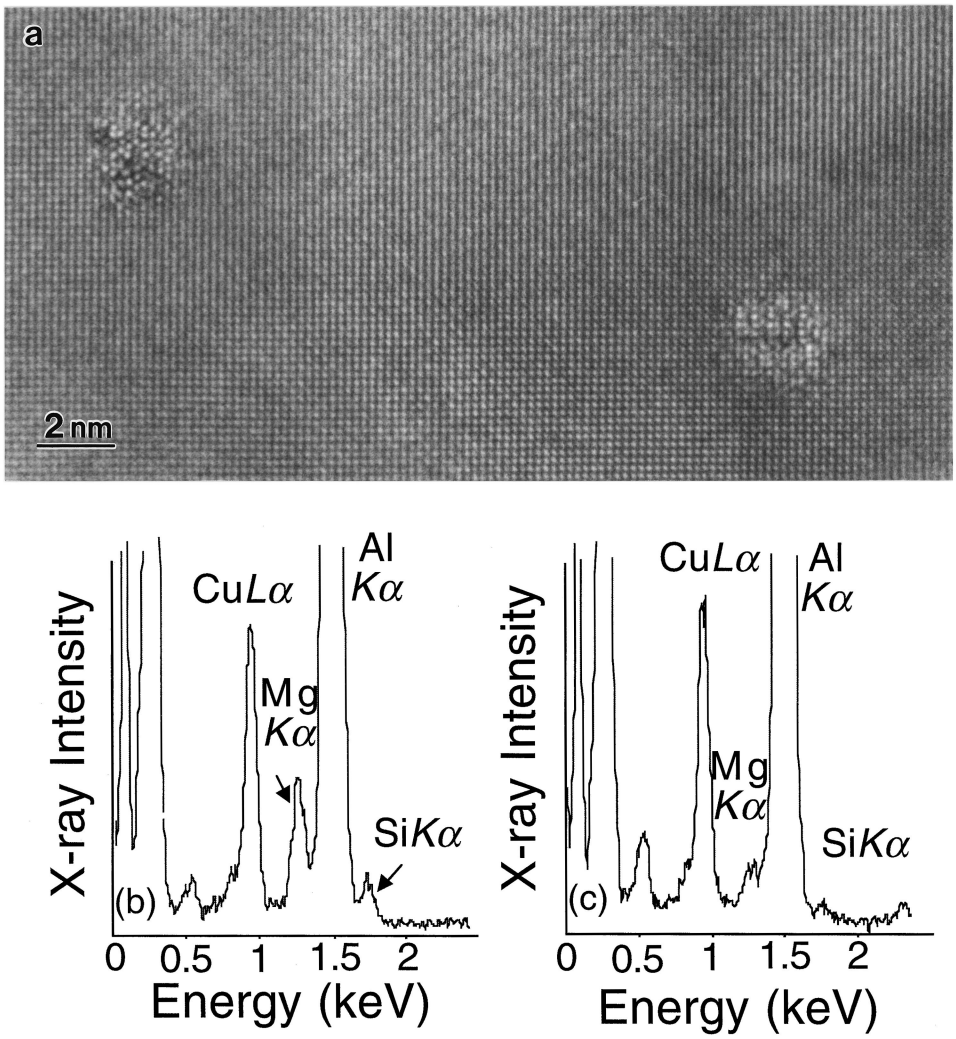

Fig. 9—(*a*) High resolution transmission electron micrograph recorded in the $\langle 001 \rangle_\alpha$ orientation from the Al-2.5Cu-1.5Mg-0.1Si (wt pct) alloy in the peak hardness condition (200 °C, 14 h). The image exhibits contrast from the GPB zone–like precipitates in the end-on orientation. Energy dispersive X-ray spectrum acquired (*b*) from within a single precipitate and (*c*) from a nearby matrix region.

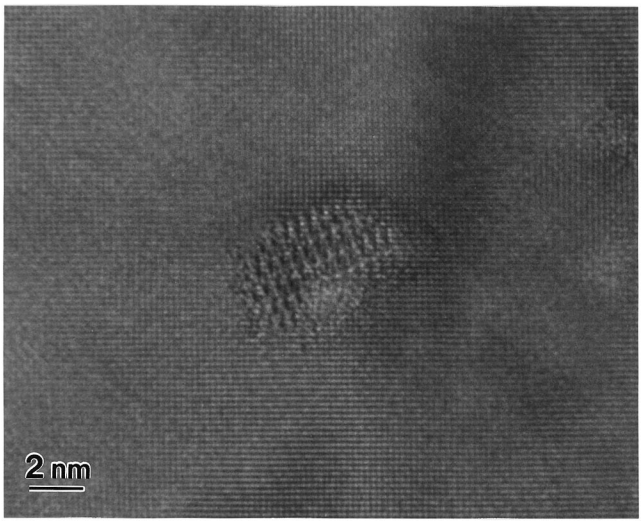

Fig. 10—High resolution transmission electron micrograph recorded in the $\langle 001 \rangle_\alpha$ orientation from the Al-2.5Cu-1.5Mg-0.25Si (wt pct) alloy in the peak hardness condition (200 °C, 14 h). The image shows a GPB zone–like in direct contact with an equilibrium S precipitate, suggestive of heterogeneous nucleation.

literature to construct an isotherm at 520 °C for this system. He used published isotherms from the Al-Mg-Si, Al-Cu-Si, and Al-Cu-Mg systems to determine the shape and position of the α solid solution field for the Al-Cu-Mg-Si phase diagram at 520 °C. The section at 1.4 wt. pct Cu and 520 °C is represented in Figure 12. Collins showed that the solid solubility of Mg and Si is not significantly altered by the amount of Cu present at 520 °C and that there was no shift in the α solid solution solvus boundary at 520 °C for alloys containing between 0.25 and 1.4 wt pct Cu.[30]

The compositions of the alloys studied in this investigation and those studied by Suzuki *et al.*[23] and Gupta *et al.*[24,25] are plotted in Figure 12 as H1-H3, S1-S2, and G1-G4, respectively. The composition of the alloys studied by Wilson and co-workers[7,19,20] and Weatherly and Nicholson[21,22] are very close to the Al-2.5Cu-1.5Mg-0.25Si wt pct (H2) alloy studied in this investigation, and for this reason, these alloys are not plotted in Figure 12. Although each of the alloys have a similar Cu/Mg ratio, the alloys with 1.5 wt pct Mg lie in a different phase field at 520 °C than those with 0.75 wt pct Mg or 0.9 wt pct Mg. Alloys H1, H2, and H3 used in the present investigation lie either in or on the solvus boundary of the (α + Mg_2Si) phase field of this isotherm.

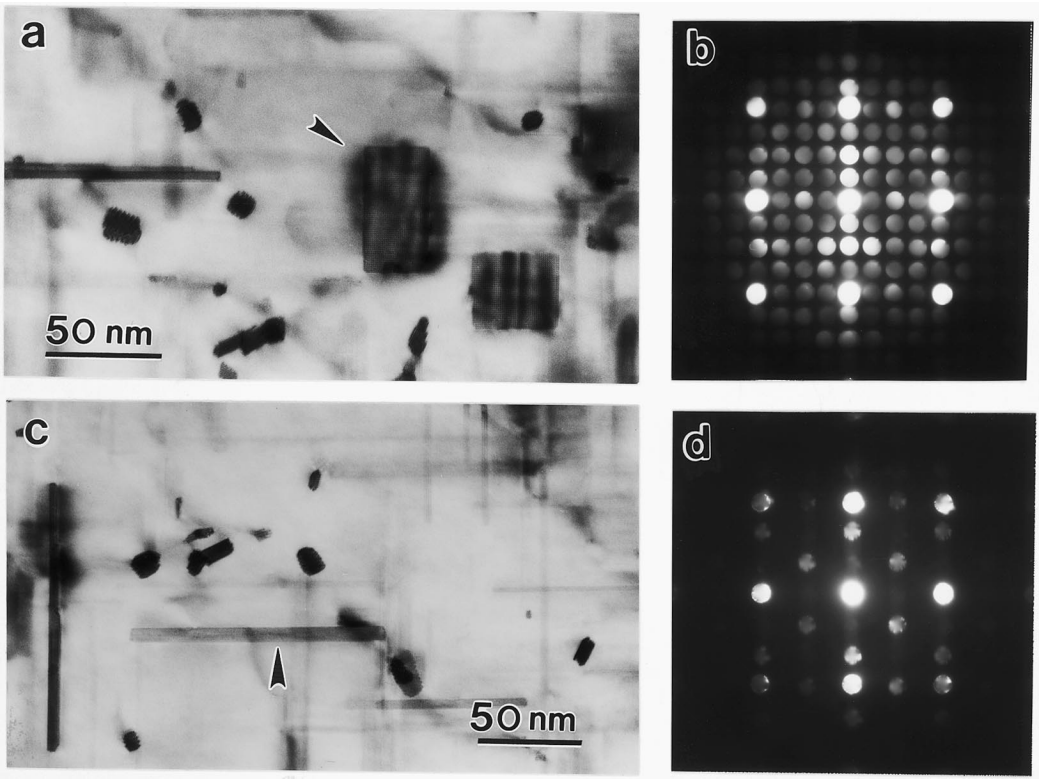

Fig. 11—Analysis of precipitates formed in Al-2.5Cu-1.5Mg-0.5Si wt pct alloy. (*a*) BF transmission electron micrograph showing cuboidal precipitates that were identified as σ phase ($Al_5Cu_6Mg_2$) by acquiring microbeam electron diffraction patterns, provided in (*b*), from individual precipitates. (*c*) BF transmission electron micrograph showing plate-shaped precipitates that were identified as θ' phase (Al_2Cu) by acquiring microbeam electron diffraction patterns, provided in (*d*), from individual precipitates.

The predictions from this isotherm are consistent with our initial tentative identification of the Mg- and Si-rich precipitates found in the AQ microstructures of the Si-containing alloys. On the basis of these observations, it is concluded that these precipitates are Mg_2Si. Suzuki *et al.* reported the presence of Mg_2Si in addition to S in the alloy Al-2Cu-0.9Mg-0.25 Si (wt pct) (S1). Figure 12 shows that the composition of alloy S1 lies very close to the $\alpha/(\alpha + Mg_2Si)$ solvus boundary, and the presence of Mg_2Si at the solution treatment temperature may be expected. Furthermore, Suzuki *et al.* reports that additions of 0.5 wt pct Si additionally promotes the formation of Q phase ($Al_5Cu_2Mg_8Si_6$). Figure 12 shows that the alloy containing 0.5 wt pct Si (S2) lies on the $(\alpha + Mg_2Si)/(\alpha + Mg_2Si + Q)$ phase boundary, and therefore, the presence of small amounts of Q phase at the solution treatment temperature may also be expected. The alloys studied by Gupta *et al.* (G1 to G4) either lie in the α-phase field (alloy G1) or the $(\alpha + Q)$ phase field (alloys G2 to G4). These predictions match very well with the experimental observations reported by Gupta *et al.* Clearly, the presence of insoluble Mg_2Si and Q phase precipitates at the solution treatment temperature will have significant, yet different, effects on the matrix solute content. In this respect, we should not necessarily expect the observations made by Gupta *et al.* to be the same as those made by Suzuki *et al.* or those made in this investigation. This analysis demonstrates that the effect of Si on the precipitation processes clearly depends not only on the Cu/Mg ratio but also on the total solute content of the alloy.

The absence of dislocation loops in the AQ microstructures of the Si-containing alloys suggests that there is a preferred interaction between the microalloying additions and vacancies. It has been reported that the vacancy binding energies for Si, Mg, and Cu are 0.7, 0.04, and 0.01 eV, respectively.[31] Following earlier proposals,[2–7] it is proposed that a reduction in free vacancy concentration in the α-Al arises from the binding between vacancies and microalloying additions, which reduces the rate of diffusion and delays the natural age-hardening response of the Si-containing alloys. This proposal is also consistent with the systematic decrease in AQ hardness values recorded with increasing Si content in the quaternary alloys. In this regard, it is also likely that the increase in the volume fraction of Mg_2Si precipitation in the AQ microstructure, with increasing Si content, would remove Mg and reduce any potential solid solution effects. Finally, it is noted that despite the absence of loops in the AQ microstructure of the Si-containing alloys, the defect density in these alloys was increased after very short exposures to elevated aging temperatures and this was also evident after prolonged natural aging (Figure 4). It is suggested that these defects are available to interact with vacancies and solute atoms and that this interaction results in the rapid hardening, as proposed recently.[6] Further work on the nature of this interaction and the hardening mechanism is required.

The present results indicate that the enhanced peak hardness associated with Si additions is due to the formation of an extremely fine and uniform distribution of a GPB zone–like precipitate. These zones contained Si and exhibited faceting on $\{001\}_\alpha$ planes. The cross-sectional morphology of these precipitates, which were elongated along $\langle 001\rangle_\alpha$ directions, varied from square rod to lath shaped as the Si content

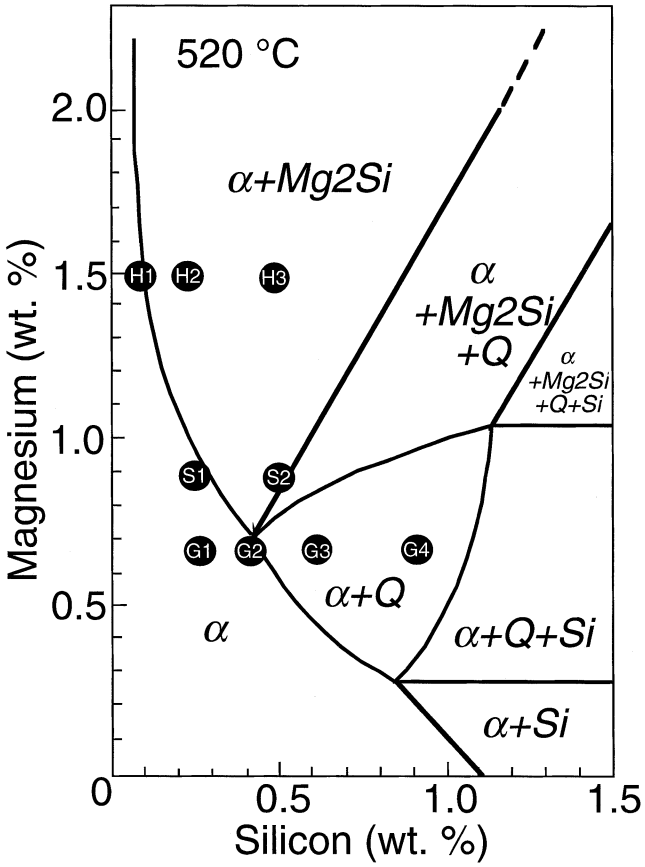

Fig. 12—Section of the isotherm of the Al-Cu-Mg-Si phase diagram at 520 °C. The composition of the Si containing alloys used in the present study are labeled H1-H3, those studied by Suzuki *et al.*[23] are labeled S1-S2 and those studied by Gupta *et al.*[24,25] are labeled G1-G4. The figure is reproduced using the data from Collins.[30]

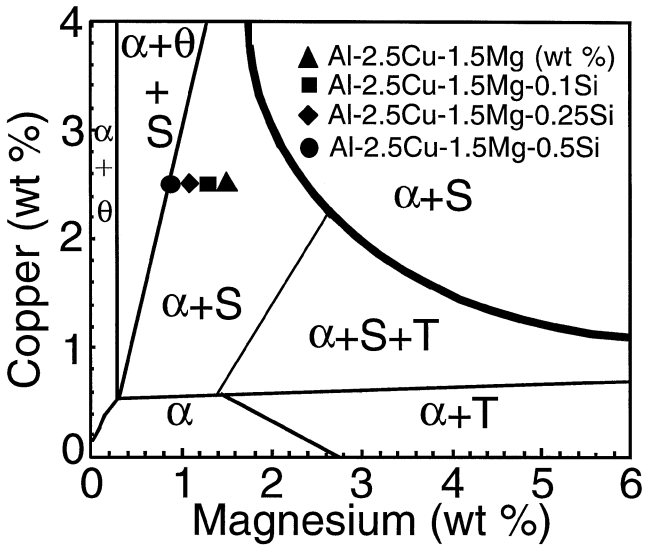

Fig. 13—Aluminum-rich corner of the Al-Cu-Mg phase diagram showing the phases present as a function of composition after long-term aging at 190 °C. The thick solid line defines the (α + *S*) phase boundary at 500 °C.[1] Also superimposed is the composition of the ternary Al-2.5Cu-1.5Mg (wt pct) alloy and the Mg composition ranges of the matrix after the addition of 0.1, 0.25, and 0.5 (wt pct) Si. The figure indicates the reduction in Mg composition of the matrix in each of the three Si-containing alloys caused by the formation of insoluble Mg_2Si at the solution treatment temperature.

increased. It is proposed that this effect on morphology is the result of elastic strains associated with the introduction of Si atoms to the zone structure. Recently, Reich *et. al.*[6] used 3DAP to examine the composition of GPB zones in an Al-Cu-Mg alloy and found that the zones contained Cu and Mg and were preceded by more diffuse co-clusters of Cu and Mg. It is proposed that similar clustering processes precede the nucleation of the Si-modified GPB zones observed in this study, such that the modified GPB zones nucleated at the site of or evolved from these clusters. A number of similar evolutionary processes involving precipitation from atomic clusters of solute have recently been reviewed.[32] These observations are contrary to previous work that attributed the increases in hardness to a refined distribution of S phase.[2,7,19–23] The presence of S phase does not appear to be the primary origin of the increased peak hardness of the Si-containing alloys. In fact, a refined dispersion of S phase precipitates was only observed in the overaged microstructure of the Si-containing alloys. The present results also indicate that the Si-modified GPB zones can act as nucleation sites for S phase, as demonstrated in Figure 10.

In Figure 13, we have evaluated the total solute content of the matrix by plotting the composition of the present alloy set on the ternary Al-Cu-Mg phase diagram after accounting for the Mg removed by the presence of the insoluble Mg_2Si particles in the AQ condition. The figure shows the Al-rich corner of Brook's Al-Cu-Mg ternary phase diagram, determined by X-ray diffraction experiments by Silcock at 190 °C and 500 °C.[1] The removal of Mg from the solid solution pushes the alloy matrix composition toward the (α + θ + S) phase field. The overaged microstructures observed for the alloys containing 0.1 and 0.25 wt pct Si contained only S phase precipitates. This is consistent with the predictions from the alloy compositions plotted in Figure 13, where it is seen that the effect of Si on the matrix compositions does not shift them outside of the (α + S) phase field. However, for the alloy containing 0.5 wt pct Si, the composition of the matrix extends to the boundary between the (α + S) and the (α + θ + S) phase fields. Therefore, it seems reasonable that we observe precipitation of metastable allomorphs of the θ phase in this higher Si alloy. A similar analysis would explain the observation of θ' (Al_2Cu) in Suzuki *et al*'s[23] Al-2Cu-0.9Mg-0.5Si (wt pct) alloy. It appears that the effect of Si on the overaged microstructures can be rationalized on the basis of the changes to the matrix composition arising from the presence of insoluble particles present at the solution treatment temperature. The observation that the volume fraction of these particles increases during aging (Table II) further accentuates this effect. The observation of the σ phase is also thought to be related to this effect and suggests that further work on the phase diagram is required.

V. CONCLUSIONS

1. The observed precipitation sequence for the Si-containing alloys at 200 °C involves

$$\text{SSSS} + Mg_2Si \rightarrow \alpha + \text{Si-modified GPB zones}$$
$$+ Mg_2Si \rightarrow \alpha + S + Mg_2Si$$

In alloys possessing higher Si contents, the precipitation of other phases is also likely.

2. The enhanced hardening associated with Si-bearing Al-Cu-Mg alloys is primarily due to the formation of a fine and uniform dispersion of Si-modified GPB zones. These zones contain Si and possess faceting along the cube planes of the matrix.
3. The addition of Si does result in a refinement of the distribution of S-phase precipitates; however, this dispersion was not observed until after peak hardness. It is suggested that the higher level of hardness during overaging in the Si-containing alloys is due to this refined dispersion of S phase. Furthermore, evidence that these precipitates can form by heterogeneous nucleation on the Si-modified GPB zones that dominate the peak hardness microstructures has been presented.
4. The previously unidentified cubic precipitate identified by Wilson[20] and Weatherly and Nicholson[21,22] in the alloys containing 0.25 wt pct Si has been found to be the σ phase ($Al_5Cu_6Mg_2$). In accordance with the results of Suzuki *et al.*,[23] the θ' precipitate also forms in higher Si content alloys. The unidentified precipitate reported by Gupta and co-workers[24,25] and Suzuki *et al.* for the alloys containing greater than 0.5 wt pct Si was not observed in this work.
5. The effect of Si on the precipitation processes depends on the total solute content of the alloy in addition to the Cu/Mg ratio. The differences in reported precipitation sequences can be reconciled to thermodynamic analyses by consideration of the effect of insoluble constituents present at the solution treatment temperature on the matrix composition.

ACKNOWLEDGMENTS

This work was partially supported by the Australian Research Council. CRH especially acknowledges the financial support of the NSF-DMR during completion of the manuscript.

REFERENCES

1. G.B. Brook: "Precipitation in Metals," Special Report No. 3, Fulmer Research Institute, Stoke Poges, United Kingdom, 1963.
2. J.T. Vietz and I.J. Polmear: *J. Inst. Met.*, 1966, vol. 94, pp. 410-19.
3. S.P. Ringer, T. Sakurai, and I.J. Polmear: *Acta Mater.*, 1997, vol. 45, pp. 3731-44.
4. S.P. Ringer, S.K. Caraher, and I.J. Polmear: *Scripta Mater.*, 1998, vol. 39, pp. 1559-67.
5. P. Ratchev, B. Verlinden, P. De Smet, and P. Van Houtte: *Acta Mater.*, 1998, vol. 46, pp. 3523-33.
6. L. Reich, S.P. Ringer, and K. Hono: *Phil. Mag. Lett. A*, 1999, vol. 79, pp. 639-48.
7. R.N. Wilson and P.G. Partridge: *Acta Metall.*, 1965, vol. 13, pp. 1321-27.
8. Y.A. Bagaryatsky: *Dokl. Akad. SSSR*, 1952, vol. 87, p. 397.
9. Y.A. Bagaryatsky: *Dokl. Akad. SSSR*, 1952, vol. 87, p. 559.
10. J.M. Silcock: *J. Inst. Met.*, 1960, vol. 89, pp. 203-10.
11. F. Cuisiat, P. Duval, and R. Graf: *Scripta Metall.*, 1984, vol. 18, pp. 1051-56.
12. A.M. Zahra, C.Y. Zahra, C. Alfonso, and A. Charai: *Scripta Mater.*, 1998, vol. 39, pp. 1555-58.
13. A.M. Zahra, C.Y. Zahra, W. Lacom, and K. Spiradek: *Proc. Int. Conf. on Light Metals*, Amsterdam, June 20–22, 1990, ASM International, Materials Park, OH, T. Khan and G. Effenberg, eds., 1990, pp. 633-39.
14. A.K. Jena, A.K. Gupta, and M.C. Chaturvedi: *Acta Metall.*, 1989, vol. 37, pp. 885-95.
15. H. Perlitz and A. Westgren: *Ark. Kemi. Miner. Geol.*, 1943, vol. 13, p. B16.
16. A.K. Gupta, P. Gaunt, and M.C. Chaturvedi: *Phil. Mag. A*, 1987, vol. 55, pp. 375-87.
17. C.B. Zhang, W. Sun, and H.Q. Ye: *Phil. Mag. Lett. A*, 1989, vol. 59, pp 265-71.
18. S.P. Ringer, K. Hono, I.J. Polmear, and T. Sakurai: *Appl. Surf. Sci.*, 1996, vols. 94–95, pp. 253-60.
19. R.N. Wilson, D.M. Moore, and P.J.E. Forsyth: *J. Inst. Met.*, 1967, vol. 95, pp. 177-83.
20. R.N. Wilson: *J. Inst. Met.*, 1969, vol. 97, pp. 80-86.
21. G.C. Weatherly and R.B. Nicholson: "Ministry of Aviation," Department of Materials, Progress Report Number PD/25/025, 1964.
22. G.C. Weatherly and R.B. Nicholson: "Ministry of Aviation," Department of Materials, Progress Report Number PD/29/025, 1965.
23. H. Suzuki, I. Araki, M. Kanno, and K. Itoi: *Trans. Jpn. Inst. Light Met.*, 1977, vol. 27, p. 239.
24. A.K. Gupta, A.K. Jena, and M.C. Chaturvedi: *Mater. Sci. Technol.*, 1987, vol. 3, pp. 1012-17.
25. A.K. Gupta, M.C. Chaturvedi, and A.K. Jena: *Mater. Sci. Technol.*, 1989, vol. 5, pp. 52-55.
26. A.K. Jena, A.K. Gupta, and M.C. Chaturvedi: *Metall. Trans. A*, 1993, vol. 24A, pp 2181-87.
27. M.C. Chaturvedi, A.K. Gupta, and A.K. Jena: *Mater. Sci. Eng.*, 1989, vol. A110, pp. 187-92.
28. T. Gladman and J.H. Woodhead: *J. Iron Steel Inst.*, 1960, Feb., pp. 189-93.
29. R.D. Schueller, A.K. Sachdev, and F.E. Wawner: *Sripta Metall.*, 1992, vol. 27, pp. 617-22.
30. D.L.W. Collins: *J. Inst. Met.*, 1958, vol. 86, pp. 325-36.
31. J. Takamura, M. Koiwa, and J. Furukawa: *J. Nucl. Mater.*, 1978, vols. 69–70, p. 738
32. S.P. Ringer and K. Hono: *Mater. Characterization*, 2000, vol. 44, pp. 101-32.